Solar Energy Materials and Solar Cells xxx (xxxx) xxx–xxx

Contents lists available at ScienceDirect

Solar Energy Materials and Solar Cells

journal homepage: www.elsevier.com/locate/solmat

Thermoelectric cooling micro-inverter for PV application

Khadija El kamouny[a,b,*], Hassane Mahmoudi[c], Brahim Lakssir[b], Abdelaaziz Nid-Bahami[b], Hassan Elmoussaoui[b], Abdelilah Benyoussef[b,c], Mohammed Hamedoun[b,**]

[a] Electrical Department, Mohammed V-Agdal University, Ecole Mohammadia d'Ingénieurs "EMI", Rabat, Morocco
[b] Moroccan Foundation for Advanced Science, Innovation and Research "MAScIR", Rabat Design Center, Avenue Mohamed El Jazouli – Madinat Al Irfane, 10100 Rabat, Morocco
[c] Academy Hassan II of Sciences and Technologies, Rabat, Ave Mohammed V, Rabat, Morocco

ARTICLE INFO

Keywords:
Power optimizer
Modular Integrated Converters (MIC)
Interleaved isolated boost converter
MPPT (Maximum Power Point Tracking)
Micro-inverter

ABSTRACT

This paper presents the design and test of a single phase and thermoelectric cooling Micro-Inverter using a DC-DC interleaved isolated boost. It focuses on the optimization of (DC-DC and DC-AC) converters performances and its physical dimensions, and presents an efficient method to track the maximum power point and the load regulation. For this purpose, a specific architecture and design of a high-reliable, robust, stable and miniaturized system are proposed.

1. Introduction

As the photovoltaic solar energy is as well promising as other renewable energies, much research and development are underway, to improve the performance of an installation. These improvements are made at the same level of PV modules manufacturing but the PV systems are less efficient because of the climatic conditions that alter their performance. For this reasons, the 'MLPEs' (Module-Level Power Electronic) include as a solution, not only to make a good harvest of the maximum power delivered by the PV, but also to adapt the DC output of the PV to the load or the grid voltage. The modules have generally a power up to 500 W. Each PV module integrates its power optimizer or Micro-Inverter that makes it more effective. The use of the multiple modules allows having a greater power if it is needed (Fig. 1).

Photovoltaic generators have a nonlinear characteristic; therefore their electrical power has a maximum that must be tracked. MPPT [1] controllers are then used for this purpose. A MPP tracker is an electronic circuit built around a DC-DC converter. DC-DC converters are mostly used for interconnections between two DC networks with different voltage levels. There are many different topologies which vary according to the complexity of circuits, stress on used components and quality of input and output power [2,3]. Generally, a single-inductor, single-switch boost converter topology and its variations exhibit a satisfactory performance in the majority of applications where the output voltage is greater than the input voltage. The performance of the boost converter can be improved by implementing a boost converter with multiple switches and/or multiple boost inductors [2]. The two inductor boost converter exhibits benefits in high power applications [3–10]: high input current is split between two inductors, thus reducing I^2R power loss in both copper windings and primary switches. Furthermore, by applying an interleaving control strategy, the input current ripple can be reduced [6]. Implementation of the topology can be in either non isolated [11] or isolated format. The isolated boost topology, which is shown in Fig. 2 [12], is attractive in applications such as power optimizer with isolation to extract the maximum power and generate high output voltage from low input voltage [11–14].

When a PV module integrates its own Micro-Inverter, its efficiency becomes more significant. Many methods are used to design Modular Integrated Converter (MIC) or also called micro-inverter. The method used in this paper to design a Micro-Inverter is based on two steps. First, the DC panel voltage is stepped up, using an interleaved isolated boost converter topology, to a much higher voltage. Then, this high DC voltage is converted into an AC signal and then filtered using an LCL filter.

The cooling of the power electronics components is ensured by using a thermoelectric model developed at MAScIR. The thermoelectric technology exploited to date by the industry is based essentially on the Peltier and Seebeck effects, the first being that which produces a heat flux from an electric current and the second one that produces an electrical voltage from a difference of heat. The generation of electricity by this new technology is based on the Seebeck effect of n and p type thermoelectric semiconductors consisting of pairs electrically connected in series and thermally in parallel by a conductive material

* Corresponding author at: Electrical Department, Mohammed V-Agdal University, Ecole Mohammadia d'Ingénieurs "EMI", Rabat, Morocco.
** Corresponding author.
E-mail addresses: k.elkamouny@gmail.com (K. El kamouny), m.hamedoun@mascir.com (M. Hamedoun).

http://dx.doi.org/10.1016/j.solmat.2017.06.061
Received 16 January 2017; Received in revised form 23 June 2017; Accepted 28 June 2017

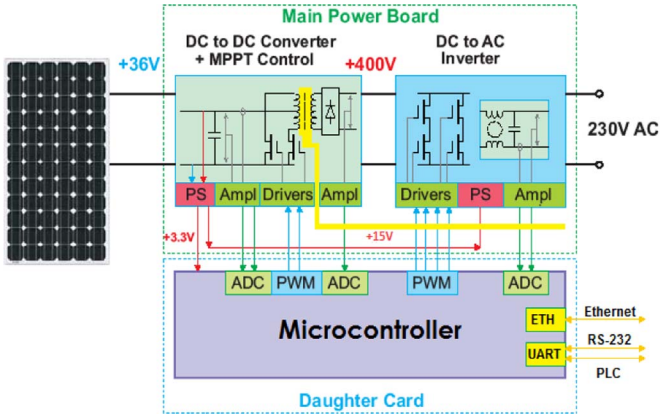

Fig. 1. Global structure of the micro-inverter.

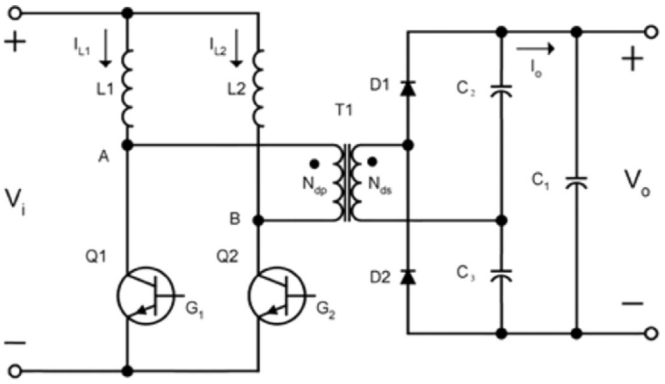

Fig. 2. Interleaved isolated boost converter.

whose thermoelectric power is assumed to be zero. The merit coefficient is given by: ZT = S2CT/K with K = Kres + Kpor, Where; S: Seebeck coefficient, K; thermal conductivity, C: electrical conductivity, ZT; merit coefficient.

In this paper the detailed information about total and local density of states of a system based on Bi2Te3 material doped with Sb and Se, will be presented, using ab-initio calculations based on full-potential linearized augmented plane wave (FP-LAPW) method, as implemented in the Wien2k code.

2. Overall architechture

The proposed micro-inverter is composed of two major parts that will be able to deliver energy to the power grid:

- The DC-DC converter used to boost the voltage of the panel (about 36 V) to reach a voltage of 400 V and is also responsible to implement the MPPT algorithm, hence the need for current sensors and voltage at the panel and its output, high efficiency and a large step-up ratio are the most important requirements.
- The DC-AC converter is an H-bridge, controlled by a PWM high frequency signal in one arm, and the same frequency signal of the electric network in the other arm. The adoption of this modulation strategy optimizes the effectiveness of Micro-Inverter with a significant reduction in switching losses. The selection of power components is crucial for the proper functioning of the topology in terms of efficiency.

The system is powered by auxiliary choppers which generate voltages of 15 V and 5 V, its boot voltage is about 18 V. A linear regulator with low dropout voltage ensures the micro-controller power. Three signals read by the micro-controller to control the system, two voltage dividers are used to detect the input and output voltage DC-DC converter. Since the micro-controller is powered from the system input side, the high-voltage bus feedback signal is opto-isolated to provide galvanic isolation between the input and the output of the system. Finally, the input current generated by the photovoltaic module is detected using a shunt current measurement. These signals are sampled by an integrated analog-digital converter in the micro-controller every 20 ms. The main features of the system are summarized in Table 1:

Table 1
Technical specifications of the micro-inverter.

Parameters	Min	Typ.	Max
Vin (input voltage)	18 V	35 V	55 V
MPPT margin	22 V	–	26 V
Iin (input current)	–	8 A	11 A
DC-DC output	–	381 V	500 V
DC-AC output	184 V	230 V	270 V
Iout (output current)	–	1 A	1.1 A
Output power	–	250 W	–
DC-DC switching	–	37.5 kHz	–
DC-AC switching	–	18.75 Hz	–

2.1. Interleaved isolated DC-DC boost

Interleaved isolated DC-DC boost converters have the goal to achieve high input voltage gain by the use of capacitor multiplier systems or high-frequency transformers [12]. However, since galvanic isolation is required for some MLPE such as Micro Inverters applications, the HF transformer is always necessary. Thus, to obtain an output voltage up to 320 V DC from a standard PV panel with a low voltage range 20–40 V, this voltage value allows to the inverter to supply the grid with the suitable regulated voltage level. The DC-DC stage is also responsible for implementing the Maximum Power Point Tracking (MPPT) which is charged of extracting maximum power from the photovoltaic module [15]. The discussed solution offers the benefit of reducing power loss in both copper windings and primary switches [16,17], as the high input current is split between two inductors. Furthermore, implementing such topology reduce significantly the input ripple current [18]. Some of the advantages of DC-DC boost converters are the increased efficiency up to 97%, reduced size of magnetic components by operating in high frequencies, faster transient response, and improved reliability (Tables 2–7).

2.1.1. Operation principle

The converter operates in continuous conduction mode (CCM) (as shown in the Fig. 2). It has four operation intervals. During the first interval, the MOSFET Q1 is ON and Q2 is OFF, the inductor L1 is charging and its current increases linearly with a slope proportional to the input DC voltage. The inductor L2 returns the stored current through the primary thus causing the transfer of energy to the secondary with some amplification. During the second interval, MOSFETs Q1 and Q2 are closed (OFF) and the inductors are charging. In that instant, the primary HF transformer is short-circuited and the load is supplied by the capacitor as shown in Fig. 2. The third interval where Q2 is ON and Q1 is OFF this case is similar to the first one except that the inductor L2 is charging while L1 is restoring its energy. The last

Table 2
Technical specifications of the DC/DC converter.

Parameters	Min	Typ.	Max
Vin (input voltage)	20 V	35 V	40 V
Power output	–	250 W	–
Vout (output voltage)	270 V	381 V	430 V
Efficiency	97%	–	–
Switching frequency	–	37.5 kHz	–

Table 3
The technical specifications of the MOSFETs chosen for the DC / DC converter.

MOSFET	IPB020N10N5
Rdson(mΩ)	2
Tswoff(ns)	77 + 29
Vbr(V)	100
Id in 25 °C (A)	120
Qg(nC)	210
Manufacter	Infineon technologies
Unit price	5.55 USA

Table 4
The technical specifications of the diodes chosen for the DC/DC converter.

Diode	VS-15EWX06FN-M3
Rf(V)	1.5 in 15 A
Trr(ns)	18
Vbr (V)	600
IF in 100 °C (A)	15
IRM in 125 °C (A)	4.6
Manufacter	Vishay semiconductor

Table 5
The technical specifications of the selected transformer.

Transformer	06100
Transformation ratio	2.66 (3%)
nominal operating frequency	35 kHz
Maximum current	4 A
Maximum power	250 W
Manufacter	Magnetica

Table 6
Technical specifications of the selected inductors.

Inductors	06103
Inductance	600 µH (15%)
Resistance	81 mΩ
Maximum current	4 A
Saturation current	6.5 A
resonant frequency	637 kHz
Manufacter	Magnetica

Table 7
MOSFET Specifications of the DC- AC converter.

MOSFET	IXFA22N65X2
Rdson (mΩ)	145
Tswoff(ns)	42 + 18
Vbr(V)	650
Id in 25 °C (A)	22
Qg(nC)	37
Manufacter	IXYS
Unit price	3.98 USA

interval where Q1 and Q2 switches are open is here avoided by taking a duty cycle greater than 50%.

2.1.2. Sizing

In the following calculation, it is assumed that the maximum duty ratio is 0.7. And since this ratio is greater than 0.5, the D ratio will be taken greater than 0.5, therefore:

$$D_{max} = \frac{t_{on_{max}}}{T_s} - 0.5 = 0.2$$

Calculation of the maximum power input:

$$P_{in_{max}} = \frac{P_{out}}{n} = \frac{250}{0.97} = 257.7\ \text{W}$$

Calculating the maximum average current:

$$I_{in_{max}} = \frac{P_{in_{max}}}{V_{in_{min}}} = \frac{257.7}{20} = 12.8\ \text{A}$$

Calculating the maximum RMS current:

$$I_{rms_{max}} = \frac{\sqrt{2-D}}{2}.\ I_{in_{max}} = \frac{\sqrt{2-0.2}}{2}.12.8 = 8.6\ \text{A}$$

Calculating the maximum average output current:

$$I_{out_{max}} = \frac{P_{out_{max}}}{V_{out_{min}}} = \frac{250}{270} = 0.93\ \text{A}$$

Calculating the transformer boost ratio:

$$\frac{N_2}{N_1} = \frac{\frac{V_{out}}{2}.(1-D)}{2.V_{in}} = \frac{\frac{380}{2}.(1-0.2)}{2.30} = 2.53$$

Knowing that Vout and Vin are the averages of the output and input voltage.minimal current calculation for the continuous conduction mode (CCM) of the chopper:

$$P_{lim} = 10\%P_{out} = 0.1.250 = 25\ \text{W}$$

$$I_{lim} = \frac{1}{2}.\ \frac{P_{lim}}{V_{in}} = \frac{1}{2}.\ \frac{25}{30} = 0.625\ \text{A}$$

Calculating the input inductors:

$$L = \frac{V_{in_{min}}.\ D_{max}}{\Delta I_{ind}.\ f_s} = 640\ \mu\text{H}$$

Knowing that $\Delta I_{ind} = I_{lim}$

RMS current calculation in diodes:

$$I_{Drms_{max}} = \sqrt{2-D}\ .\ \frac{I_{in_{max}}}{2.n} = \sqrt{2-0.2}\ .\ \frac{12.8}{2.2.6} = 3.3\ \text{A}$$

Where n is the elevation ratio of the selected transformer. Calculating the output capacity:

$$C \geq \frac{I_0.\ D.\ T_s}{\Delta V_{max}} = \frac{0.675.0.2.28.57.10^{-6}}{0.2} = 1.92\ \mu\text{F}$$

Calculating of the Maximum ESR output capacity:

$$\Delta I_{cap} = \frac{I_{in}}{2.n} = 2.4\ \text{A}$$

$$ESR_{cap_{max}} = \frac{\Delta V_{max}}{\Delta I_{cap}} = \frac{0.2}{2.4} = 83.3\ \text{m}\Omega$$

Calculating the breakdown voltage of the MOSFET:

$$V_{brdw} \geq 1.2.\frac{V_{out_{max}}}{2.n} = \frac{430}{2.2.6} = 99.2\ \text{V}$$

Calculating the breakdown voltage of the diodes:

$$V_{brdw} \geq 1.2.V_{out_{max}} = 1.2.430 = 516\ \text{V}$$

Calculating the input capacity:

$$C_{in} = \frac{\Delta i_c}{37500.\Delta V_c} = \frac{0.675}{37500.2} = 9\ \mu\text{F}$$

$$ESR_{max_{C_{in}}} = \frac{\Delta V_c}{\Delta i_c} = \frac{2}{0.675} = 2.96\ \Omega$$

Calculating the power dissipation of the MOSFET:

$$P_{sw_{max}} = \frac{V_{ds_{max}}.\ I_{d_{max}}.\ t_{sw_{off}}}{2.T_s} = \frac{100.\frac{12.86}{2}.\ (77+29).\ 10^{-9}}{2.26.67.10^{-6}} = 1.27\ \text{W}$$

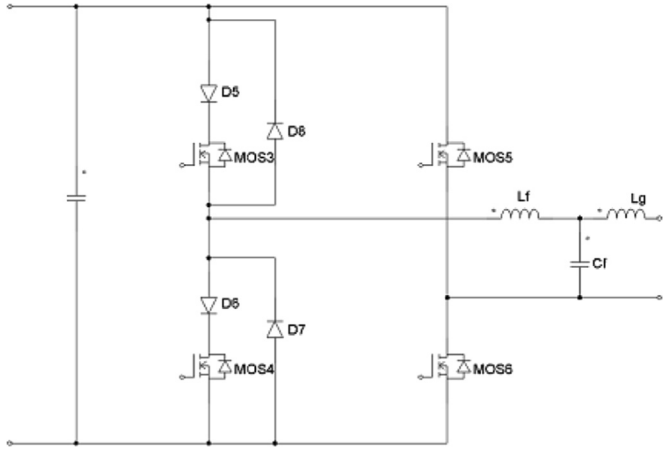

Fig. 3. Basic scheme of a DC-AC converter.

$$P_{cond_{max}} = 1.6.R_{dson}.\ I^2{}_{rms} = 1.6.2.10^{-3}.\ 8.6^2 = 0.23\ \text{W}$$

$$P_{drv} = V_{gs}.\ Q_g.\ f_s = 15.210.10^{-9}.37500 = 0.11\ \text{W}$$

$$P_{tot} = 2.P_{sw_{max}} + 2.P_{cond_{max}} + 2.P_{drv} = 3.22\ \text{W}$$

Calculation of the dissipation of the diode:

$$P_{sw_{max}} = \frac{1}{2}\frac{V_{brdwn}.\ I_{rm}.\ t_{rr}}{T_s} = \frac{1}{2}\frac{600.4.6.18.10^{-9}}{26.67.10^{-6}} = 0.93\ \text{W}$$

$$P_{cond_{max}} = 1.16.I_{avg} + 0.053.I^2{}_{Frms} = 1.16.0.675 + 0.053.3.2^2 = 1.3\ \text{W}$$

$$P_{tot} = 2.P_{sw_{max}} + 2.P_{cond_{max}} = 4.46\ \text{W}$$

2.2. DC/AC converter: single phase inverter

The basic diagram of a DC/AC converter controlled using a 3 levels PWM signal presented in Fig. 3. MOS3 and MOS4 are controlled by the PWM signal modulated to give the sinusoidal shape with a frequency of 18.75 kHz. Schottky diodes are connected to the drain of the two MOSFETs to disable their internal diodes. The other two external diodes are connected in anti-parallel to replace the free-wheeling diodes to prevent reverse recovery problems MOSFETs. MOS5 and MOS6 are controlled by a single frequency square wave 50 Hz. The LCL filter is connected to the output of the bridge for interfacing the load. In the input of the converter there is an output capacitor for storing and supplying energy on demand.

The minimum value required for the input capacitance is:

$$C_{bus} = \frac{4.P_{out}}{V^2{}_{bus_{max}}}.\ t_1 = \frac{4.250.5.10^{-3}}{370^2} = 36.52\ \mu\text{F}$$

t_1 is given by:

$$t_1 = \frac{1}{4.F_{grid}} = 5\ \text{ms}$$

The value of L_F is chosen to limit the current ripple to 20% of rated current. The following equation allows the calculation of this value:

$$L_f = \frac{1}{n}.\ \frac{\left(V_{bus} - V_{grid_{pk}}\right).\ D}{\Delta i.\ f_{sw}} = \frac{1}{3}.\ \frac{(380 - 325).0.75}{0.22.18750} = 33.33\ \text{mH}$$

Where n is the number of level control ($+ V_{bus}$, and $- V_{bus}$, 0). The value of the capacitor C_f is selected to limit the exchange of reactive power to 5% of the nominal power.

$$P_{reactive} < 0.05.P_{active}$$

$$X_{Cf} \geq \frac{V^2{}_{grid}}{0.05.P_{active}} = \frac{230^2}{12.5} = 4232\Omega$$

$$C_f = \frac{1}{\omega.\ X_{C_f}} = 750\ \text{nF}$$

To prevent the filter resonance effect with the low and high harmonics, the resonance frequency should be between the frequency of the line divided by 10 and half of the changeover frequency. The resonant frequency of an LCL filter is:

$$f_{res} = \frac{1}{2.\pi}\sqrt{\frac{L_f + L_g}{L_f.\ L_g.\ C_f}}$$

By choosing Cf = 470 nF and the coupling inductance is equal to the inductance of the filter Lg = Lf, a resonant frequency is obtained: fres = 5.4 kHz that respects constraints mentioned earlier. 4 selected MOSFETs of the bridge are:

2.3. Embedded software

Using MCF52230 has several advantages including the availability of several PWM “Pulse Width Modulation” channels to control converters, enough of ADC channels to measure voltages and currents, UART modules used for PLC “Power Line Communication”, DMA and Timer modules to facilitate internal management, and an Ethernet module as another alternative for communication.

The program residing in the micro-controller is mainly divided into two parts. The first part is the communication of the state and the measured values to the server. The second periodic part with the highest priority will manage the behavior of Micro-Inverter. Figure shows the machine status of the micro-inverter.

2.3.1. Management of micro-inverter

The first sub program allows to the Micro-Inverter to perform its main function, adapt and deliver the energy produced by the photovoltaic panel. For this, the micro-inverter starts by initializing peripherals, and check the input voltage.

If it complies with its specifications, it starts slowly charging its internal capabilities through the DC-DC converter to avoid draining the current suddenly causing the voltage drop at the input. After reaching the allowed margin of the bus voltage, it starts the DC-AC converter; the relay closes and engages the load, eventually moving to performing the MPPT algorithm and the periodic inspection of devices.

The second sub-program is the program of communication. It was limited at first time to use Ethernet communication. No important change for migrating to the PLC support. This sub program starts by making an attempt to connect to the server, if the attempt fails the micro-inverter restarts again after a fixed waiting period. If the connection is established, the micro-inverter will wait for request to execute and return a response if necessary. The defined commands are presented in Table 8 any other unrecognized command, the micro-inverter does not respond.

2.4. Thermoelectric cooling system

The bismuth telluride is a narrow – layer semiconductor with a regional unit cell. The structure of the valence and conduction band can be described as a multiple ellipsoid model with 6 constant energy ellipsoids centered on the reflection planes. Bi2Te3 easily connects along the regional axis because of the Van der Waals interaction between neighbouring tellurium atoms. Because of this, the bismuth telluride materials used for production or cooling applications must be polycrystalline. In addition, the Seebeck coefficient of Bi2Te3 is compensated around the ambient temperature, forcing the materials used in the energy production devices to be an alloy of bismuth, antimony, tellurium and selenium (Figs. 4 and 5).

In this part, we use the ab-initio calculations based on full-potential linearized augmented plane wave (FP-LAPW) method, as implemented in the Wien2k code [17]. This method employing the generalized

Table 8
Requests and signification.

Requests	Significations
WHO AM I (wh)	Return the answer "Micro-Inverter" so the Server can identify the client.
GET MI INFO (mi)	Returns the Micro-Inverter information: the manufacturer, part number, serial number, hardware and software versions, and the date of conception.
GET MI SPEC (sp)	Returns the specification of the micro-inverter: maximum power, the MPPT range, the range of the output voltage, maximum current …
GET STAT (gs)	Returns the current state of the micro-inverter: the current phase, the voltages of the panel and the bus, the current panel and power consumption, the state of the relay …
GRID DISCONNECT (gd)	Forces the micro-inverter to disconnect from the grid.
GRID CONNECT (gc)	Allows micro-inverter to connect to the grid.
RESTART (rs)	Requests the micro-inverter to restart its software.

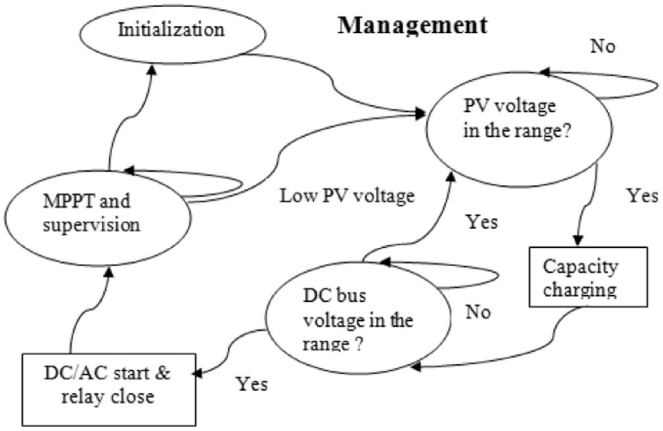

Fig. 4. Synoptic operating micro-inverter/management.

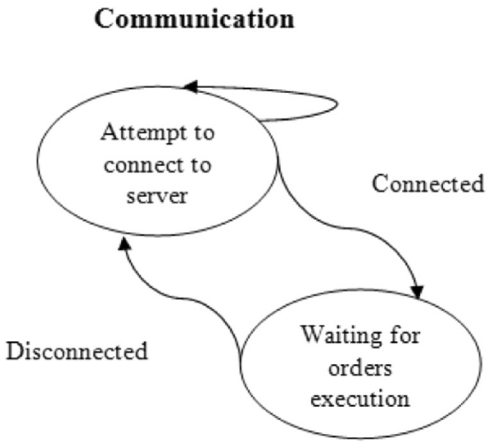

Fig. 5. Synoptic operating micro-inverter/communication.

gradient approximation (GGA) [18], also we use BoltzTraP code for calcul thermoelectric properties.

The Fig. 6 shows the crystal structure of the bulk Bi2Te3. It has a Rhomboedric symmetry which can be described by the space group *R*-3*m* (N°166), with the lattice parameters a = 4.38 Å, c = 30.47 Å and the atomic positions of Bi(0, 0, 0.399); Te1at (0, 0, 0); and Te2at (0, 0, 0.2069) [19].

The calculated spin orbit coupling band structures of Bi2Te3 shows in Fig. 7 for both methods GGA and mBj. The Fermi level set at 0 eV with the dash lines. It is clear that the band structures show a semiconductor behavior with band gap close to 0.149 and 0.27 eV respectively. The minimum of the conduction band and the maximum of valence band are both at R. So, this material is making a direct band gap.

In Fig. 8, the partial density of states shows that the S orbital's of the two types of atoms of tellurium contribute most states of the conduction bands and the p orbital's of the two types of atoms of tellurium

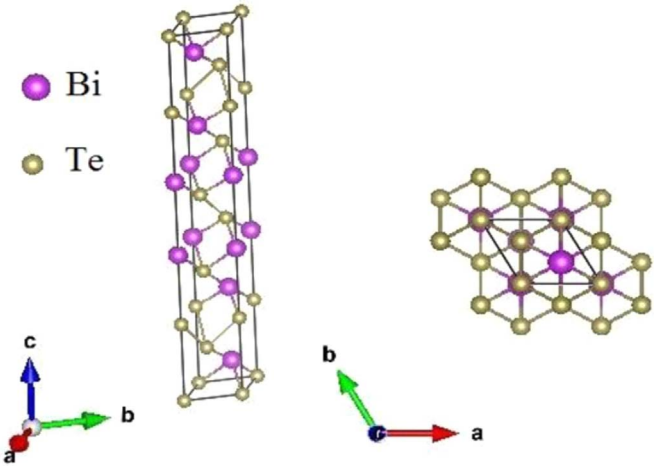

Fig. 6. Crystal structure of bulk Bi2Te3.

contribute most states in the valence bands. P orbital's of bismuth atoms contribute most to the conduction band and most of the orbital S bismuth states contribute to the conduction band, but not as much as tellurium atoms.

The result of gap energy (Table 9) of Bi2Te3 doped with Sb and Se become type P and type N, respectively.

The majority of the thermoelectric materials are bulk based Bi2Te3 used at temperature (300 K) with a high figure of merit. In the case of p-type, this is the substitution of bismuth with Sb that allows obtaining the Bi2-xSbxTe3 composition. The substitution of tellurium to Se in turn allows obtaining the n-type composition Bi2Te3-xSex. So, the result of thermoelectric properties shows that doped Bi_2Te_3material with Sb and Se respectively (Figs. 9–11).

The theoretical value of the Seebeck coefficient for n-Type and p-Type Bi2-xSbxTe3 are presented in Table 10, which are in good agreement with value obtained from the experimental Seebeck coefficient at 300 K [20]. However, it is shown that for p-Type Bi1.65Sb0.35Te3 the seebeck coefficient of 228.02 is better than that obtained in referance.

3. Practical results

After assembling the demonstration board of the micro-inverter some tests was performed on the different parts, including power supplies, sensors voltages and current, DC-DC and DC-AC converters. These tests are preliminary; they don't justify the actual performance of the micro-inverter.

The main demonstration board consists of two electronic boards:

- Electronic power board, It includes the three main parts: the DC-DC and the DC-AC converter and the filter circuit.
- Electronic control board or a daughter board: it includes all systems that manage and control the Micro-Inverter, it consists of three main circuits and programs: The MPPT program, Power Line

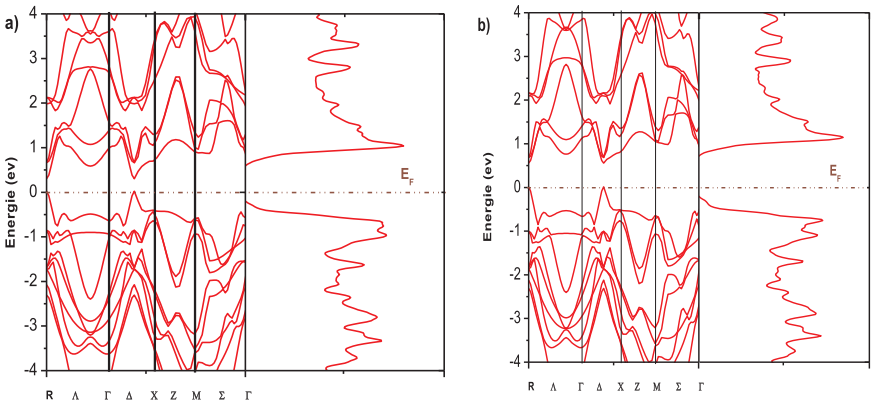

Fig. 7. Band structures and Total Dos of bulk computed using a) the GGA and b) the mBj approximation functional with spin orbit coupling.

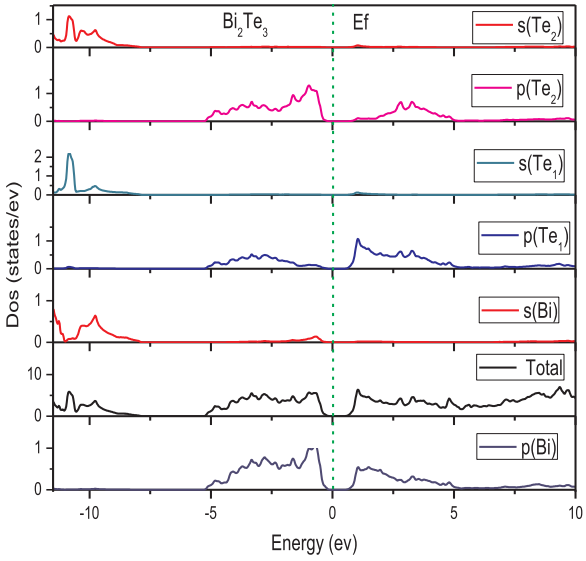

Fig. 8. The partial and total density of the bulk Bi2Te3.

Table 9
Material type with its theoretical gap energy.

compound	Type	Gap theoretical energy (eV)
$Bi_2Te_{2.25}Se_{0.75}$	n-Type	0.153
$Bi_2Te_{1.5}Se_{1.5}$	n-Type	0.103
$Bi_{1.66}Sb_{0.33}Te_3$	p-Type	0.144
$Bi_{1.33}Sb_{0.66}Te_3$	p-Type	0.122
Bi_2Te_3	–	0.149
Bi_2Se_3	–	0.221
$Bi_1Sb_1Te_3$	P-Type	0.126

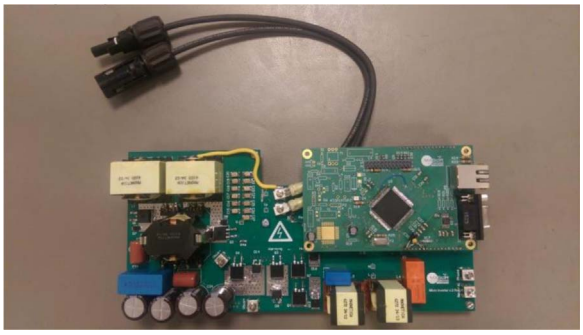

Fig. 9. Demonstration board of the micro-inverter/top view.

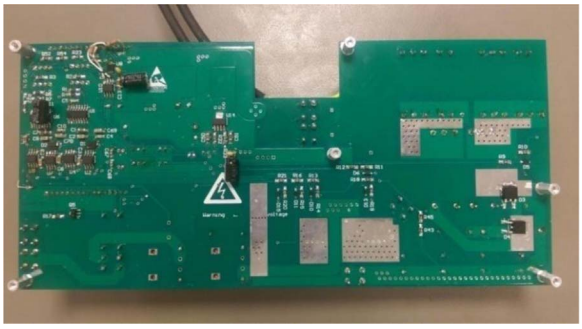

Fig. 10. Demonstration board of the micro-inverter/bottom view.

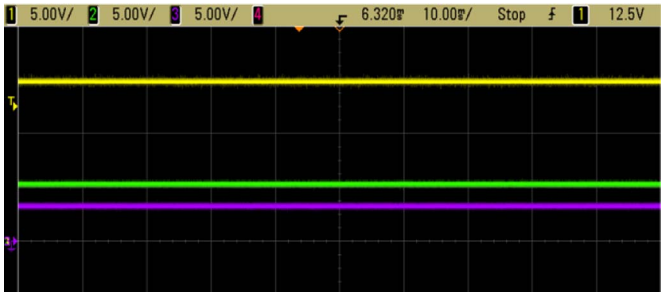

Fig. 11. The supply voltages 3.3 V, 5 V and 15 V.

Table 10
The values of Seebeck coefficient depending on the concentration of doping x for n-Type and p-Type Bi2-xSbxTe3 at 300 K.

Compounds	Type	Seebeck coefficient (μV/K) theories	Seebeck coefficient (μV/K) experimental
Bi2Te2.25Se0.75	n-Type	− 192.05	− 208 (Bi2Te2.75Se0.3) [20]
Bi2Te1.5Se1.5	n-Type	− 169.03	–
Bi1.65Sb0.35Te3	p-Type	228.02	–
Bi1.35Sb0.65Te3	p-Type	211.97	210 (Bi0.5Sb1.5Te3) [20]

Communication program PLC and Ethernet/supervision program.

3.1. Power supplies

Fig. 12 shows the non isolated supply voltages. The micro-inverter powered by the photovoltaic panel.

The isolated power supplies must be measured with the second reference. The Fig. 12 shows the test results.

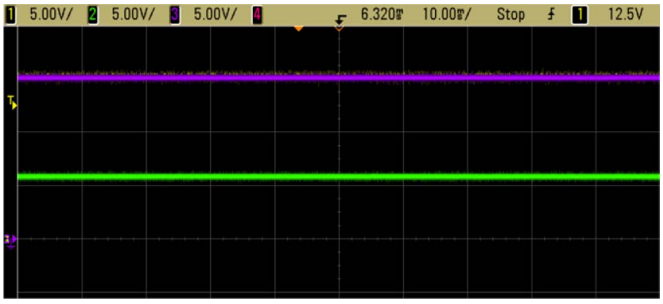

Fig. 12. The isolated supply voltages 5 V and 15 V.

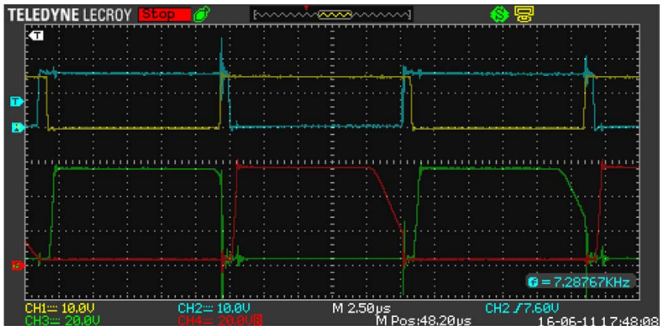

Fig. 13. The voltages of the gate and drain of the MOSFETs DC-DC.

3.2. DC-DC converter: practical results

The control voltages of the MOSFETs (DC-DC) are shown in Fig. 13 yellow and blue, and their Vds voltages in green and red respectively.

In a single-phase PV system, power flowing to the grid varies over time, while the PV power must be constant to use the maximum energy from PV panel, otherwise this can result an input power mismatch with the generated output power. Therefore, a decoupling or storage component must be placed in the system to balance this possible mismatch between the input and output power. In two stage topologies, a decoupling capacitor bank is placed between the DC-DC and DC-AC stages. Thin-film capacitors are used on the DC-bus to improve long-term system reliability. In order to have DC bus voltage that is higher than the peak of grid voltage during the whole sine period, the minimum capacitor value can be calculated.

The value of DC bus decoupling capacitance was calculated to be 88 µF (Four capacitance of 22 µF in parallel) and verified in the system

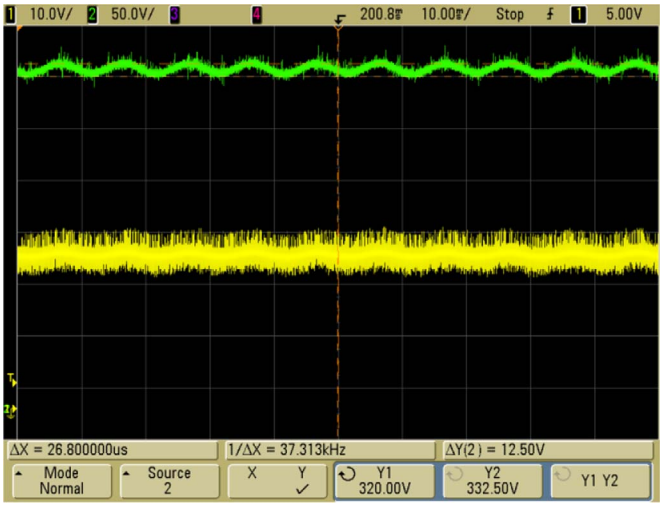

Fig. 14. Voltage ripple in DC-DC converter output. (For interpretation of the references to color in this figure legend, the reader is referred to the web version of this article.)

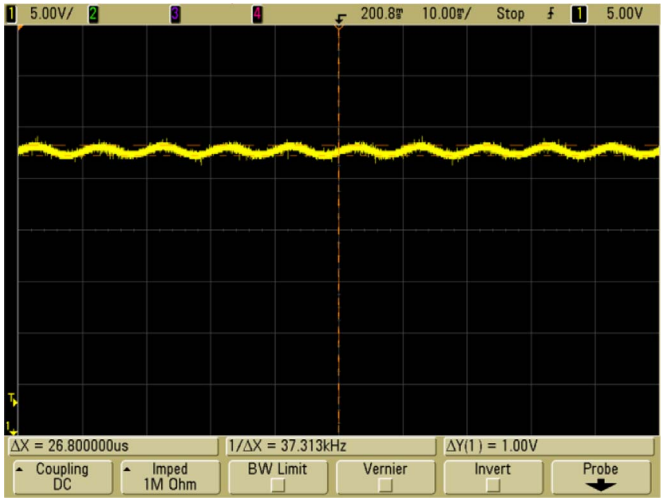

Fig. 15. Voltage ripple in DC-DC converter input.

as sufficient. If large voltage ripples are present on the DC link voltage, a DC bus ripple elimination algorithm was successfully implemented and tested. The voltage ripple in the output of the DC-DC converter is less than 4% (12.50 V) as is shown in the Figs. 14 and 15.

The measurements made using this system gave excellent results:

- Total harmonic distortion (THD) is below 3%.
- MPP tracking efficiency reached 99.5%.
- Demo efficiency was found to be 93.

A capacitance of 13 µF is also placed in the input of the DC-DC converter to filter the PV voltage and the PV voltage ripple is equal to 1 V.

3.3. DC-AC converter: practical results

As previously mentioned, the DC-AC converter requires two modulation frequencies, the first one is 18.75 kHz and the second is the frequency (50 Hz). Fig. 15 shows the signals generated by the microcontroller and sent to the driver that will regenerate two complementary signals from each received signal and apply them to the gates of H bridge MOSFETs.

Before obtaining the desired result, a problem has been appeared at that converter. The temperature of the high frequency MOSFETs began to increase very quickly, something that was abnormal. The first step is performed to put the reference to the oscilloscope GND, the first probe (green) in point VS, the second probe (blue) to the bottom MOSFET gate (VG2), and the third probe (yellow) VDD voltage. The test result is given in Fig. 16. The signals are as expected; the bottom part is functioning normally.

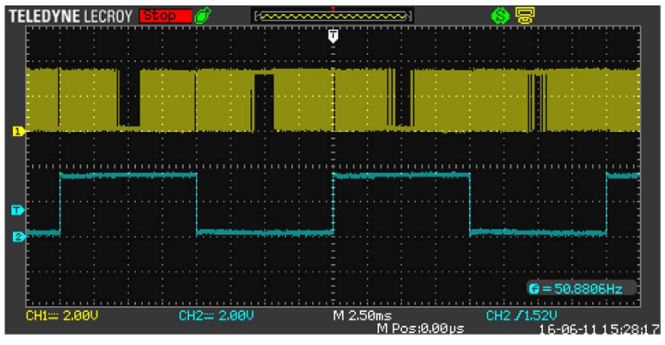

Fig. 16. Control signals of the DC-AC converter. (For interpretation of the references to color in this figure legend, the reader is referred to the web version of this article.)

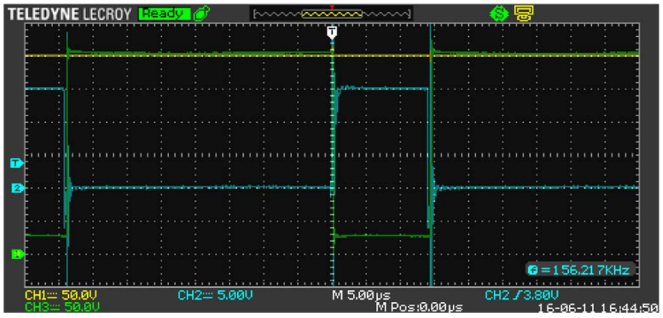

Fig. 17. The test results from the bottom part of the high frequency arm. (For interpretation of the references to color in this figure legend, the reader is referred to the web version of this article.)

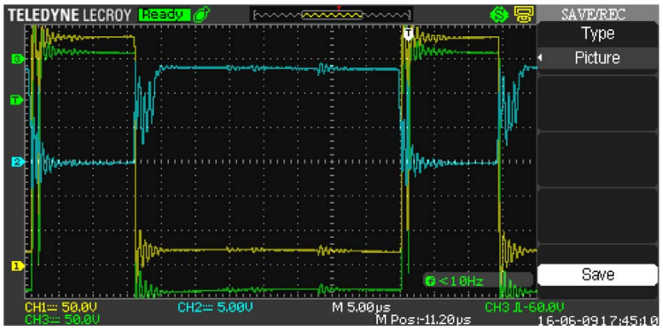

Fig. 18. The test results from the bottom part of the high frequency arm. (For interpretation of the references to color in this figure legend, the reader is referred to the web version of this article.)

The top part is tested by placing the reference to point VS, the first probe (Yellow) to the bus voltage, the second probe (blue) in the gate of the top MOSFET VG1 and the third probe to GND (Fig. 17).

Fig. 18 shows the result of the measurement, where some oscillations at this level. This oscillation is generated by the driver (blue signal) mainly in the transition from the ON state to the OFF one. At this level (Fig. 18), we note that because of oscillations, the top MOSFET supposed be blocked (OFF) turns on (ON) for a short time (250 ns) which drops the voltage in the bus bypassing the reference. At that moment, a strong current goes through both MOSFETs causing the temperature increase.

This problem was solved by replacing the failed driver, giving an improved result. The oscillation found in each transition (Fig. 19) is called "MOSFET gate ringing", which is due to the inductive effect generated by the length of the tracks. This inductive effect accompanied by the external resistance of the gate and its internal capacity gives rise to an oscillatory RLC circuit (Figs. 20).

Because of the unavailability of a high voltage probe, the 3 screen taken in Fig. 22 shows the output voltage of the micro-inverter.

Fig. 23 shows the unfiltered output voltage of the DC-AC converter at rated voltage with the frequency spectrum. Note the presence of

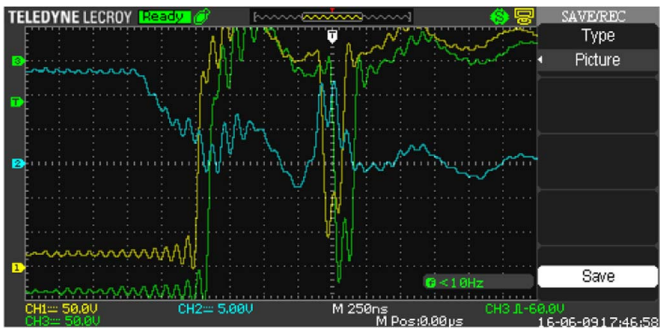

Fig. 19. The test results of the bottom part of the high frequency arm (zoomed).

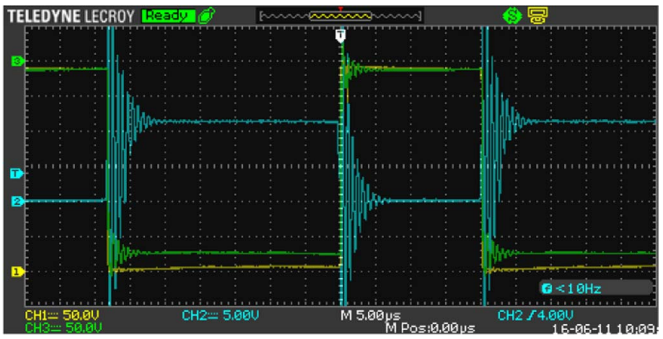

Fig. 20. The test results from the bottom part of the high frequency arm after solving the problem.

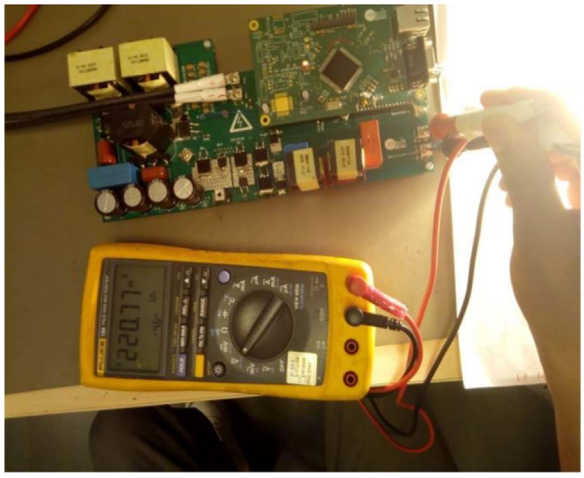

Fig. 21. Output voltage of the micro-inverter measurement.

several harmonics including that of 18.75 kHz. These harmonics are almost filtered by the LCL filter (Fig. 24), harmonic remains can be noticed in the sine wave (Fig. 25).

As already mentioned, the DC-AC converter has a hybrid modulation allowing one leg to switch at 18.75 kHz and one leg to switch at grid frequency. The image in Fig. 15 is a scope capture of the two modulating signals generated by the microcontroller and sent to the input pin of the driver. This device is then used to generate the two complementary signals controlling the gate of each MOSFET in the bridge.

The resulting output voltage waveforms are shown in Fig. 21. Output voltage on the filter the efficiency of the system has been measured connecting the Micro-Inverter to a resistive. Load and adapting the ohmic value of the electrical load to the desired output power level.

3.4. Thermal parameters analysis

Before doing infrared camera test, a simulation was done, using COMSOL platform, to demonstrate the temperature profile or thermal distribution the Fig. 26, presents the propagation of the temperature through the plate in an ambient temperature environment equal to 25 °C and the Fig. 27 shows the temperature propagation in temperature ambient of 40 °C using a standard heatsink.

The heating of the Mosfet transistor, when the system is in continuous operation for many hours, is reported in the Fig. 28. The temperature of the Mosfet reaches 77.9 °C. (The image in Fig. 28 was taken using an infrared camera) (Figs. 29 and 30).

The operation of the micro-inverter system without radiator, for a few hours, caused a Mosfets heating up to 77.9 °C and especially those that operate in high frequency as is shown in Fig. 28. After placing the

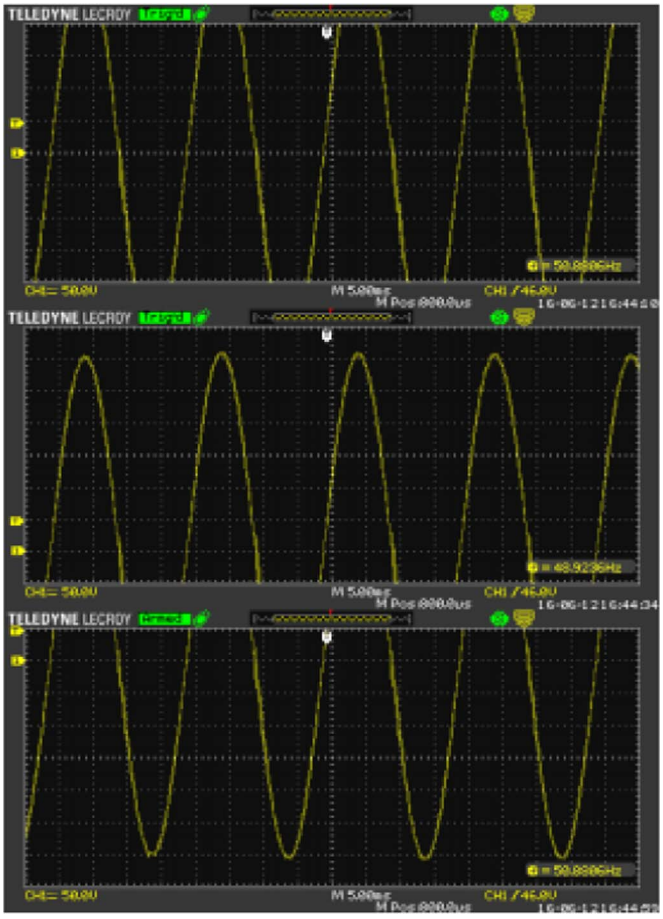

Fig. 22. The filtered output of the micro-inverter.

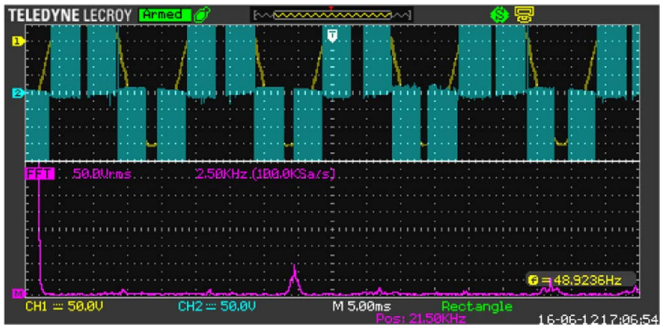

Fig. 23. The unfiltered output of the DC-AC.

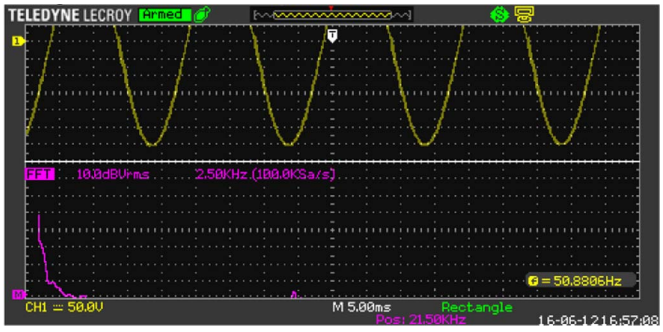

Fig. 24. The filtered output of the DC/AC.

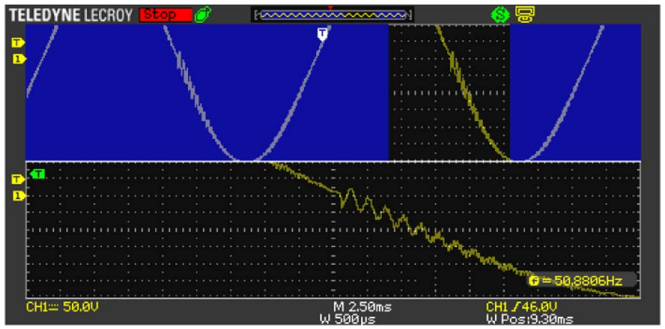

Fig. 25. The presence of harmonics in the sinusoidal.

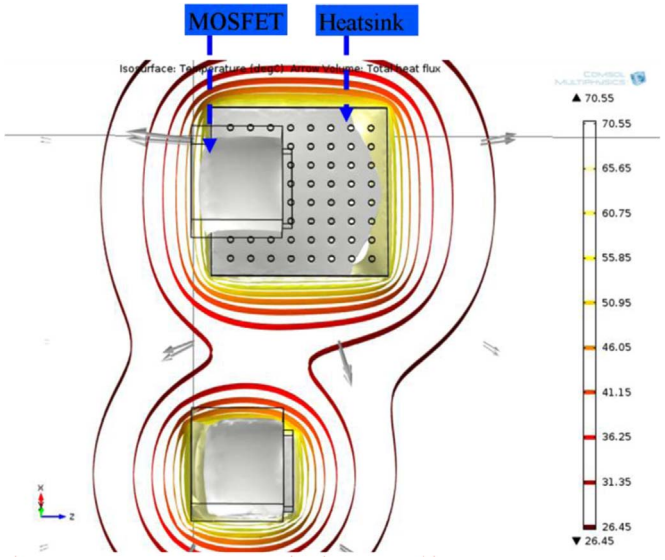

Fig. 26. Temperature propagation in 25 °C ambient temperature.

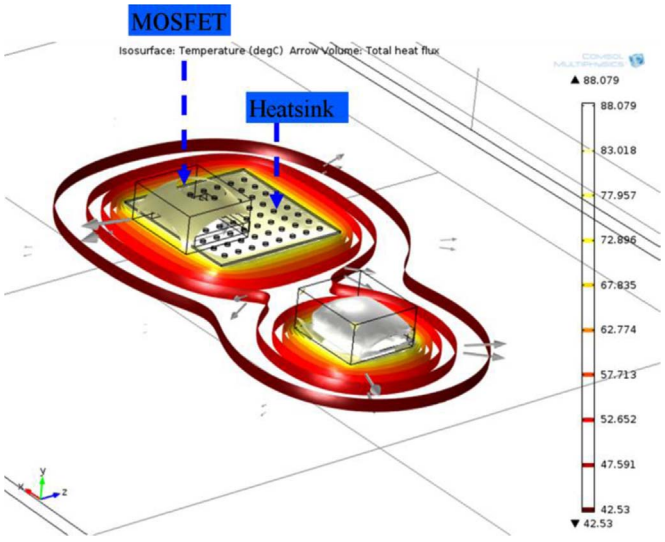

Fig. 27. Temperature propagation in 40 °C ambient temperature.

thermoelectric module in contact with the relevant Mosfet, its temperature dropped rapidly to reach the value 35 °C in a few seconds and it continues to fall to stabilize in 27 °C as is shown in Fig. 31. The thermoelectric module specifications are presented in Table 11. The efficiency of the used module is equal to 58%.

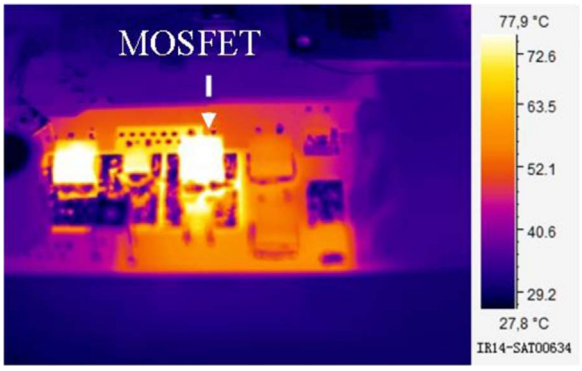

Fig. 28. Mosfet without thermoelectric module.

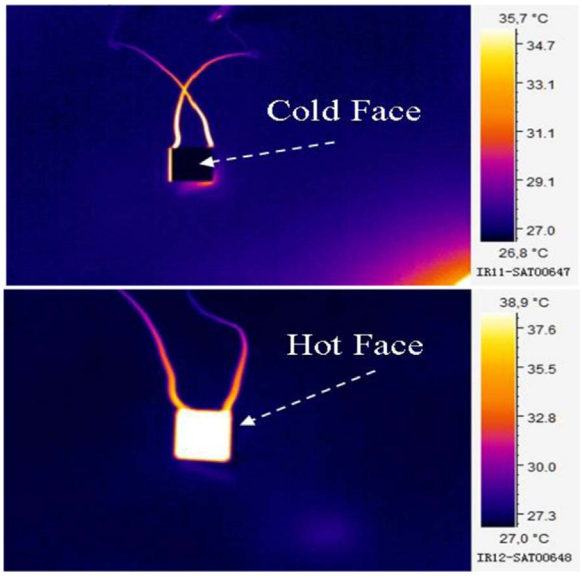

Fig. 29. Cold and Hot face of the thermoelectric cooling module.

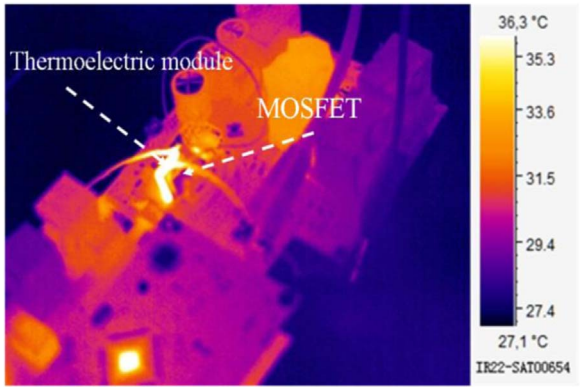

Fig. 30. The temperature of the Mosfet after using thermoelectric module.

4. Conclusion

During the design of the present Micro-Inverter, specific ferrite cores were developed and tested to be used for the power inductors and the high frequency transformer, this material improves the system performances, efficiency and reduces its physical dimensions. A particular attention was also given to the cooling process of the main power electronic components used in the system such as power transistors, power diodes and regulators, the used cooling process is based on the development and use of a thermo electrical material with a specific doping and design.

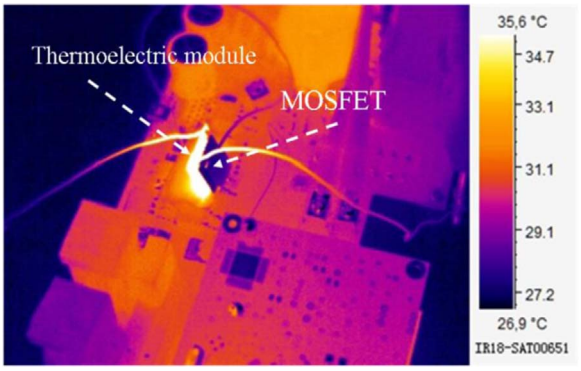

Fig. 31. Mosfet with thermoelectric module after some seconds of system shutdown.

Table 11
Specifications of thermoelectric module.

Internal resistance	1.76 Ω
I max	2 A
V max	3.8 V
Qmax	4.4 W
ΔT max	73 °C
External depth	4.8 mm
External length	15 mm

The interleaved Boost chopper is an appropriate solution for PV modules with relatively low voltage and called to supply loads at high voltages. The implementation of this structure has reduced losses through the power components, to reduce the size and weight of magnetic circuits for operating in high frequency, introducing an impedance matching for harvesting optimal power and isolate electrically the PV from the load to protect it. The main obstacle of the circuit in Fig. 2 is its limited power regulation range. Inductor L1 must support input voltage when-ever Q1 turns on. Likewise, this is true for L2 and Q2. Since the minimum duty ratio of each switch is 0.5, the magnetizing currents of the two inductors cannot be limited. This leads to a minimum output power level. If the load demands less power than this minimum level, the output voltage increases abnormally because excessive energy has been stored in the inductors.

Acknowledgments

A.K. acknowledges the financial support from IRESEN Moroccan Public Agency.

A.K. acknowledges the support from Moroccan Foundation for Advanced Science, Innovation and Research.

A.K. acknowledges this project was gold medallist in international innovation and invention competition "iCan 2016" held in Toronto Canada.

References

[1] N. Kasa, T. Iida, H. Iwamoto, Maximum power point tracking with capacitor identifier for photovoltaic power system, in: IEEE Proceedings Electr. Power Appl., vol. 147(6), 2000, pp. 497–502.
[2] T. Shimizu, N. Nakamura, K. Wada, A novel flyback-type utility interactive inverter for AC module systems, ICPE'01 (2001) 518–522.
[3] G. Kishor, D. Subbarayudu, S. Sivanagaraju, Comparison of full bridge and two inductors boost converter system, J. Theor. Appl. Inf. Technol. 34 (2) (2011).
[4] B.A. Miwa, D.M. Otten, M.F. Schlecht, High efficiency power factor correction using interleaving techniques, in: Prloc. IEEE APEC'92 Conference, 1992,pp. 557–568.
[5] J.W.Kolar, G.R.Kamath, N.Mohan, F.C.Zach, Self adjusting input current ripple cancellation of coupled parallel connected hysteresis controlled boost power factor correctors, in: Proceedings IEEE PESC'95 Conference, 1995, pp. 164–173.
[6] M.S.Elmore, Input current ripple cancellation in synchronized, parallel connected critically continuous boost converters, in: Proceedings IEEE APEC'96 Conference, 1996, pp. 152–158.
[7] J.R. Pinheiro, H.A. Grundling, D.L.R. Vidor, J.E. Baggio, Control strategy of an

interleaved boost power factor correction converter, in: Proc. IEEE PESC'99 Conf., 1999, pp.137–142.
[8] H.A.C. Braga, I. Barbi, A3-kW unity-power-factor rectifier based on a two-cell boost converter using a new parallel-connection technique, IEEE Trans. Power Electron 14 (1) (1999) 209–217.
[9] B.T.Irving, Y.Jang, M.M.Jovanovic, A comparative study of soft-switched CCM boost rectifiers and interleaved variable-frequency DCM boost rectifier, in: Proceedings IEEE APEC'00 Conference, 2000, pp. 171–177.
[10] A.V.D.Bossche, V.Valtchev, J.Ghijselen, J.Melkebeek, Two-phase zero-voltage switching boost converter for medium power applications, in: Proceedings IEEE Industry Applications Soc. Annu.Meeting, New Orleans, LA, 1998, pp. 1546–1553.
[11] M.T.Zhang, Y.Jiang, F.C. Lee, M.M.Jovanovic, Single-phase three-level boost power factor correction converter, in: Proceedings IEEE APEC'95 Conference, 1995, pp. 434–439.
[12] Liang Yan, Brad Lehman, An integrated magnetic isolated two-inductor boost converter: analysis, design and experimentation, IEEE Trans. Power Electron. 20 (2) (2005).
[13] Y.Jang, M.M.Jovanovic, New two-inductor boost converter with auxiliary transformer, in: Proceedings IEEE APEC'02 Conf, 2002, pp. 654–660.
[14] Y.Jang, M.M.Jovanovic, Two-Inductor Boost Converter, U.S. Patent 6239584, May 29, 2001.
[15] M. HUANG Bin, DAVAT Bernard, Convertisseurs continu:continu à rapport de transformation élevé pour application pile à combustible", Thèse, soutenue publiquement le 14 mais, 2009.
[16] S. Zahra Mirbagheri, Saad Mekhilef, S. Mohsen Mirhassani, MPPT with Inc.Cond method using conventional interleaved boost converter, Mediterranean Green Energy Forum 2013 (MGEF-13) Energy procedia.
[17] Yannick LOUVRIER, Etude et optimisation d'un convertisseur DC-DC à canaux multiples entrelacés, thèse NO 4718, 2010.
[18] Mounica Ganta, Pallam reddy Nirupa, Thimmadi Akshitha, Dr.R. Seyezhai, Simple and efficient implementation of two-phase interleaved boost converter for renewable energy source, Int. J. Emerg. Technol. Adv. Eng. 2 (4) (2012).
[19] (a) P. Hohenberg, W. Kohn, Phys. Rev, 136 (1964) B864;
(b) W. Kohn, L. Sham, J. Phys. Rev. 140 (1965) A1133.
[20] A.H. Li, M. Shahbazi, S.H. Zhou, G.X. Wang, C. Zhang, P. Jood, G. Peleckis, et al., Electronic structure and thermoelectric properties of Bi2Te3 crystals and graphene-doped Bi2Te3 (octobre), Thin Solid Films 518 (24) (2010) e57–e60, http://dx.doi.org/10.1016/j.tsf.2010.03.124.